Results in Physics 16 (2020) 103123

Contents lists available at ScienceDirect

Results in Physics

journal homepage: www.elsevier.com/locate/rinp

Q-switched fiber laser based on CdS quantum dots as a saturable absorber

N.M. Radzi[a], A.A. Latif[a,*], M.F. Ismail[b], J.Y.C. Liew[a,c], E. Wang[a], H.K. Lee[a], N. Tamcheck[a], N.A. Awang[d], F. Ahmad[e], M.K. Halimah[a], H. Ahmad[b]

[a] Department of Physics, Faculty of Science, Universiti Putra Malaysia, 43400 UPM Serdang, Selangor, Malaysia
[b] Photonics Research Centre, University of Malaya, 50603 Kuala Lumpur, Malaysia
[c] Institute of Advanced Technology, Universiti Putra Malaysia, 43400 UPM Serdang, Selangor, Malaysia
[d] Optical Fiber Laser Technology (OpFLAT) Focus Group, Department of Physics and Chemistry, Faculty of Applied Sciences and Technology, Universiti Tun Hussein Onn Malaysia, 84600 Pagoh, Johor, Malaysia
[e] Malaysia-Japan International Institute of Technology, Universiti Teknologi Malaysia, Jalan Sultan Yahya Petra, 54100 Kuala Lumpur, Malaysia

ABSTRACT

In this work, a Q-switched fiber laser is demonstrated using quantum dots (QDs) cadmium sulfide (CdS) as a saturable absorber (SA) in an erbium-doped fiber laser (EDFL) system. The QD CdS is synthesized via the microwave hydrothermal assisted method and embedded into polyvinyl alcohol (PVA). The QD CdS/PVA matrix film is sandwiched in between two fiber ferrules by a fiber adapter. The generation of Q-switched fiber laser having a repetition rate, a pulse width, and a peak-to-peak pulse duration of 75.19 kHz, 1.27 μs, and 13.32 μs, respectively. The maximum output power of 3.82 mW and maximum pulse energy of 50.8 nJ are obtained at the maximum pump power of 145.9 mW. The proposed design may add to the alternative material of Q-switched fiber laser generation, which gives a high stability output performance by using quantum dots material as a saturable absorber.

Introduction

Pulsed fiber laser has captured much attention where it is profoundly attractive in some specific applications such as spectroscopy [1], fiber-based sensors [2,3], biomedical research [4] and miniaturized-scale-machining [5]. Generally, pulsed laser output exhibits a smoother, sharper, accurate, and more precise penetration depth compared to a continuous wave primarily to be utilized for optical sensor and laser cutting applications. Based on these demands, analysts are actively looking for methods to produce a better quality laser output, with various techniques, and one of them is through the generation of Q-switched fiber lasers [6]. Q-switched fiber lasers are pulsed lasers with a high energy content that has been widely applied in various commercial applications. Q-switching is generally a better way of generating pulses since it is easier to induce the pulsed laser as compared to mode-locking, which would require a delicate balancing between the dispersion and nonlinearities in the laser system. There are several ways to achieve Q-switched fiber laser output either by a real saturable absorber (SA) such as semiconductor saturable absorber mirror (SESAM) [7,8] or by artificial SA such as nonlinear polarization rotation (NPR) [9], nonlinear optical loop mirror (NOLM) [10] and nonlinear amplifying loop mirror (NALM) [11]. Regardless of how SESAM is one of the most extensively used devices for generating pulsed fiber laser output, it encounters a couple of issues, including undersized bandwidth range, low threshold damage, tedious fabrication procedures, and having a significant cost of fabrication [12].

Meanwhile, artificial SA causes continuous maintenance and requires complicated adjustment in the fiber cavity configuration to establish the absorption-emission mechanism. These limitations have led to ongoing research to substitute the older approach to an alternative technique that has a wider operating range, which is by incorporating materials called as saturable absorber (SA) [13]. The uniqueness of the SA materials becomes even more apparent when the researchers discovered that certain materials own their saturation absorption ability that can improve the pulse laser quality. Thus, this technique has been considered as an effective way of obtaining energetic pulses from a laser cavity by modulating the intracavity losses using the SAs.

The generation of passively Q-switched fibers lasers have been widely explored with nanomaterials such as one-dimensional (1D) material which is carbon nanotubes (CNTs) [14,15], two-dimensional material such as graphene [16–18], black phosphorus [19,20], topological insulators(TI) [21–23], transition metal dichalcogenides (TMDs) [24–26], metal nanoparticles [27–29], and Xenes [30]. CNTs and graphene are favorable materials in the pulsed laser generation due to their low cost of production, easy to install, and operate at broad bandwidth. However, the CNT diameter distribution affects the absorption bands, which normally lead to uncontrollable non-saturable loss [31]. Graphene operates at a wider operation bandwidth as compared to CNT

* Corresponding author.
E-mail address: amirahlatif@upm.edu.my (A.A. Latif).

https://doi.org/10.1016/j.rinp.2020.103123
Received 11 January 2020; Received in revised form 2 April 2020; Accepted 16 April 2020
Available online 20 April 2020

due to zero bandgap, but it has irrational low modulation depth owing to complex precision layer engineering and doping control [32]. Black phosphorus (BP) and transition metal dichalcogenides (TMD) have captured much attention after the discovery of graphene SA; however, BP utilization as SA was unstable and tended to get easily damaged due to its hydrophilic feature when disclosed to the atmosphere [33]. TMD has a wide bandgap, which caused a limitation in the infrared wavelength working region. Compared with the two-dimensional materials described, metal nanoparticles have the advantages of variable surface plasmon resonance peak and larger nonlinear third-order coefficient [27–29] while Xenes encounter pulse energy limitation [30]. Thus, it is a great significance to expand more research in new potential material as SA.

Recently, semiconductor quantum dots (QD), another group of nanomaterial SAs have triggered rapid growing interest due to their unique electronic and optical properties. QD is classified as an ultrasmall particle in the form of a nanometer scale and falls under zero-dimensional (0D) class material [34]. QD is widely exploited in semiconductor applications such as solar cells [35], photodetectors [36], light-emitting diode (LED) [37], and transistors [38] because of their strong confinement of electrons and holes [34]. Quantum dots have the distinct advantages with large and tunable nonlinear absorption capability [39], cost-effective [40], and low saturable absorption intensity [41] compared to the low dimensional materials. Their small size distributions cause them to have a higher surface area to volume ratio, which leads to higher saturable absorption properties. This is proven by Xu [42], where QDs exhibit lower saturable intensity compared to bulk material, which is having a similar modulation depth. Lower saturation intensity proved that the QD has better saturable absorption properties and may be considered as another choice of SA device. Generally, QDs are a combination of elements from Group IV-VI, such as lead sulfide (PbS) [43–45] and II-VI, such as cadmium selenide (CdSe) [46–48], with reference to the periodic table. They are fabricated either only core or core/shell, such as reported by Ming et al. [49]. Cover-coating core/shell benefits for improving the optical stability of quantum dots [50]. However, the preparation of core/shell QDs requires a particular procedure, and the thickness of the existing shell leads to a larger average diameter size. Lately, Group IV-VI and II-VI QDs are introduced as SAs in the fiber laser system in the infrared region. They are reported to have a higher optical gain, more constant of the extinction coefficient value, better photochemical stability, and more significant Stoke shift [51].

Moreover, QDs materials encourage high optical nonlinearity that benefits in fiber laser performances such as cadmium sulfide. Cadmium sulfide is one of a semiconducting material that can be applied in photonic applications since it shows excellent performance in terms of its optical properties [52]. Thus, the existence of CdS in the fiber laser system can be compared with other QDs materials in terms of their output performances. Nanoparticles have been synthesized by different methods either by hydrothermal [53], inverse micelle [54], wet chemical [55], sol-gel [56], or solvothermal techniques [42]. Each method presents their respective advantages, such as high-temperature resistance, environmentally friendly, and high structural strength. To the best of our knowledge, none are detailing on CdS QDs operating in the infrared region. However, numerous researches run CdS QD at green light emission laser due to high absorption at visible range [57]. In this experiment, the synthesized CdS QD is embedded into polyvinyl alcohol (PVA) as a matrix film and being applied as the SA device.

The fiber laser system operates via gain media such as erbium-doped fiber (EDF) [43,44], ytterbium-doped fiber (YDF) [46], and other rare-earth-doped fiber. Q-switched pulses could have a peak-to-peak pulse duration in the region of microseconds, the average power of about a few of Miliwatts, and a repetition rate in the region of kHz, which mostly depends on the injected power. The most common way to ensure a stable Q-switching is by preserving the most straightforward method, which is the sandwiching method [46,47], where nanomaterials were sandwiched between two fiber ferrules. There are other methods of material based SA, such as D-shaped side-polished fiber and microfiber [43]. It is believed that D-shape fiber and microfiber can increase nonlinear interaction length via the evanescent field. However, there is a need for a compact, inexpensive, and efficient method to enhance the performances of the pulsed fiber laser.

In this paper, we proposed the first passively Q-switched erbium-doped fiber laser based on QD CdS/PVA matrix film as an SA in the C-band region. The QD CdS is synthesized via the microwave-assisted hydrothermal method and embedded with PVA to form a QD CdS/PVA matrix film, which to the best of our knowledge, none are detailing on CdS QD operating in the infrared region. The obtained pulsed successfully recorded with pulse repetition rate, pulse width, peak-to-peak pulse duration, and average output power of 75.19 kHz, 1.27 μs, 13.32 μs, and 3.82 mW, respectively.

QD CdS synthesis and characterization

CdS quantum dots have been prepared through a microwave-assisted hydrothermal method using Monowave 400 (Anton Paar). The raw materials being used to synthesis CdS QD are cadmium chloride ($CdCl_2$ 95%, HmbG chemicals), sodium citrate ($Na_2C_6H_5O_7$, 99–100% BDH Chemicals Ltd), sodium tetraborate ($Na_2B_4O_7$, 98–100% BDH Chemicals Ltd), sodium sulfide (Na_2S 60–62%, HmbG chemicals), L-Glutathione reduced GSH ($C_{10}H_{17}N_3O_6S$ 98%, Sigma-Aldrich). All chemicals were of analytical grade without further purification. In order to synthesize CdS QD, sodium citrate and sodium tetraborate are dissolved in the distilled water under the stirring conditions for five minutes to produce borax citrate buffer. Then, the mixture solution of $CdCl_2$, GSH, and Na_2S is added dropwisely into the borax citrate buffer solution and is stirred for 20 min. The mixture is then transferred into a glass vial and heated using a microwave reactor at 150 °C for one minute. The CdS quantum dots are then blended with the polyvinyl alcohol (PVA) to form CdS/PVA matrix film for saturable absorption testing, referring to Koteswararao [58]. Firstly, 30 wt% PVA is added into 10 ml distilled water. The mixture is then heated at 60 °C for 40 min under the stirring condition for five minutes duration. Next, 0.5 ml of CdS QD is added dropwisely into the mixture under the stirring condition for 5 min. Finally, the mixture is poured into a petri dish and dried at 40 °C for 24 h to form the matrix film. The resulted CdS/PVA matrix film is then ready to be characterized and applied in laser configuration as an SA device.

A UV–visible spectrometer characterized the linear absorption properties of the CdS/PVA matrix film is as illustrated in Fig. 1(a). The spectrum proved that the erbium-doped fiber laser system at 1562 nm could be integrated with CdS quantum dots material that works as SA, with a high peak of absorption at 1568 nm. The size of the CdS QDs is measured using a nanosizer (Malvern Nano S). The diameter size range of CdS QDs is illustrated in Fig. 1(b). The spectrum shows only one peak, which indicates it is a monomodal sample. It is found that the size of the synthesized CdS QDs is ranging from 2.3 nm to 11.7 nm. Most of the particles are in the diameter size of around 4.85 nm. It can be observed that the dominant size of the synthesized CdS QDs is less than 7 nm. The average diameter size of the CdS QDs is around (5.8 ± 0.3) nm.

Fig. 2 illustrates the images of the CdS/PVA matrix film using a high-resolution transmission electron microscope (HRTEM) under 20 nm and 10 nm resolution being characterized by JEM-2100F Field Emission Electron Microscope with an acceleration voltage of 200 kV and with 500 k of magnification.

The measurement method for the characterization of nonlinear absorption properties of the QD CdS/PVA matrix film called the twin detector method is as portrayed in Fig. 3. The configuration setup to measure the modulation depth for QD CdS thin film is assembled by using the Menlo system erbium femtosecond laser module (ELMO) as a simple mode-locked laser cavity with repetition rate and pulse width of

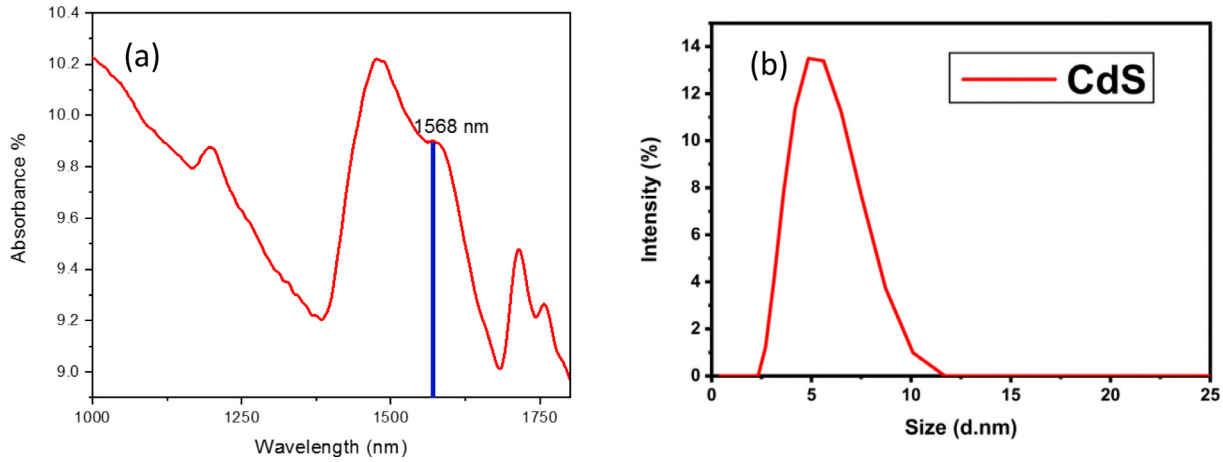

Fig. 1. (a) The linear absorption properties of CdS/PVA matrix film at a wavelength from 1000 to 1800 nm and (b) The diameter size range of CdS QDs.

100 MHz and 2.88 ps, respectively. The ELMO is controlled by a computer that allows the signal to pass through a YOKOGAWA AQ2201 variable optical attenuator (VOA) before splitting them into two equal laser beams via a 3 dB coupler. The two equal outputs of the laser beams are then connected to Thorlabs PM320E dual-channel optical power meters (OPMs). The first output acts as a reference arm without the presence of SA is denoted as OPM1. The other one of the laser beam is arranged with QD CdS-SA inserted between the path (denoted by OPM2). A series of data of output powers are recorded simultaneously for both outputs concurrently, while the attenuator loss decreases. The input laser intensity and the variation of the deviations are shown to be correlated to each other.

The experimental data of the material saturable absorption is shown in Fig. 4, where the dotted mark represents the experimental value for the modulation depth of the CdS/PVA matrix film. In contrast, the linear line represents the fitting curve based on the characterization of the modulation depth for the twin detector method. The calculated values of α_0, $I_{sat,}$ and α_{ns}, can be obtained using a formula based on previous work [59],

$$\alpha(I) = \frac{\alpha_0}{1 + \frac{I}{I_{sat}}} + \alpha_{ns} \quad (1)$$

where α(I) is the intensity-dependent absorption coefficient, α_0 is the modulation depth, I_{sat} is the saturation intensity, and α_{ns} is the non-saturable absorption loss. From the fitting, the modulation depth, saturation intensity, and non-saturable absorption loss of the device are estimated to be 19%, 0.157 MW/cm^{2,} and 81%, respectively. This indicates that CdS thin film has a robust saturable absorption property and comparable to other QDs materials.

Fiber laser configuration

The experimental setup of Q-switched fiber laser using a QD CdS/PVA matrix thin film is shown in Fig. 5. The configuration includes a laser diode (LD), a wavelength division multiplexer (WDM), an erbium-doped fiber (EDF), an isolator (ISO), a 3 dB optical coupler and a QD CdS/PVA matrix thin film as saturable absorber (SA) working in a ring cavity configuration. The LD acts as a 980 nm pump source that is injected into this cavity through 980/1550 nm WDM and followed by 3 m of an erbium-doped fiber as a gain medium. The isolator ensures that the signal only propagates in one direction without reflecting in the laser cavity. The SA consists of two fiber ferrules by sandwiching the CdS/PVA matrix thin film between them. This ring cavity consists of a 3 m Erbium-doped fiber with Group velocity dispersion (GVD) of 64 ps^2km^{-1} and a 7.01 m standard SMF (SMF-28) with anomalous GVD = -24 ps^2km^{-1}. The total net dispersion of the ring cavity is 0.024 ps^2. A 90:10 coupler is used to tap 10% of the lasing to be analyzed, and another 90% will oscillate back into the cavity. The 10% output are analyzed through a Yokogawa AQ6370C Optical Spectrum Analyser (OSA), a RTM3002 Oscilloscope, a FPC-1000 Radio-Frequency Spectrum Analyser (RFSA) and an optical power meter (OPM). The oscilloscope is used to measure the pulse repetition rate and pulse width from the displayed pulse train while OSA as an analyzer to monitor the spectrum from the cavity and RFSA to generated radio-frequency

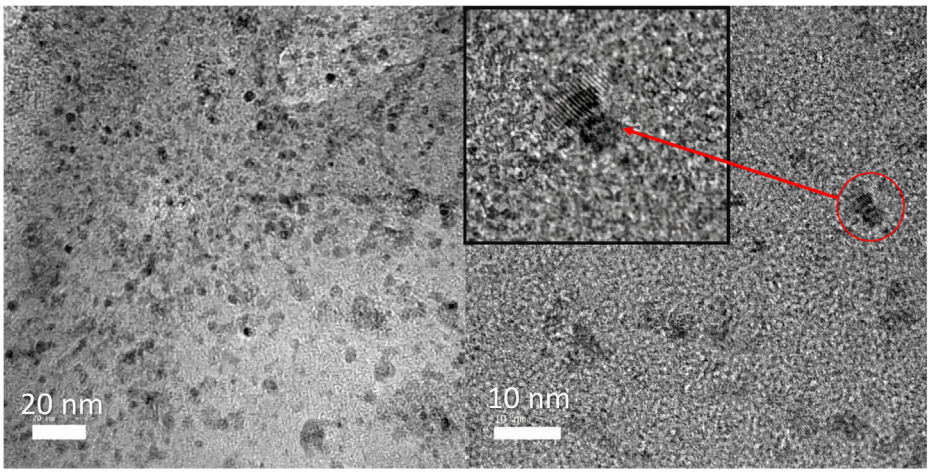

Fig. 2. The HRTEM images of the CdS quantum dots.

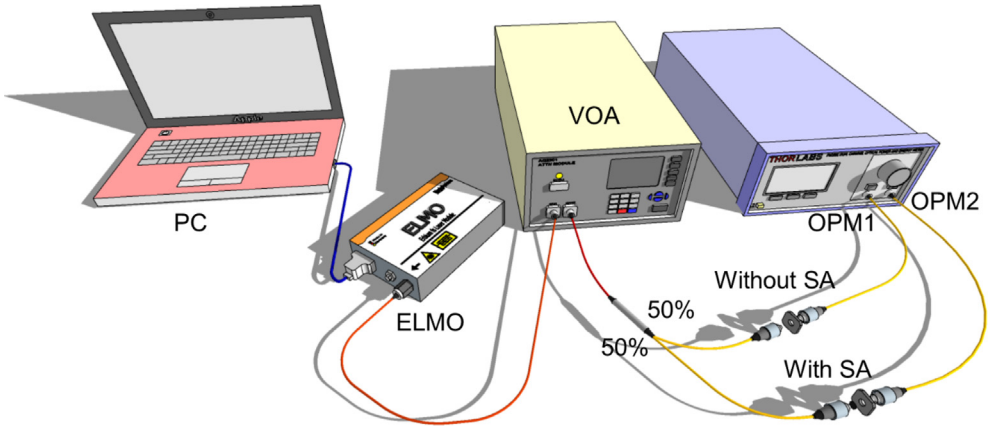

Fig. 3. The measurement setup for the modulation depth of the CdS/PVA matrix film.

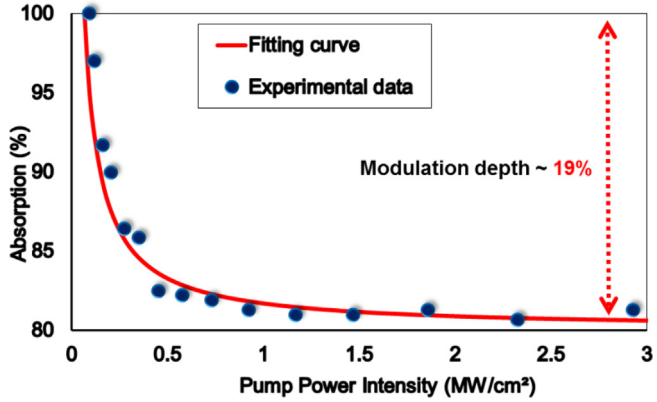

Fig. 4. Measured saturable absorption data and its corresponding fitting curve for the CdS/PVA matrix film as SA.

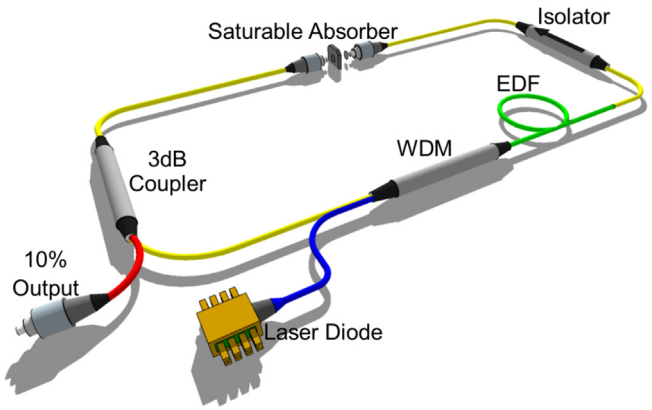

Fig. 5. Configuration setup for Q-switched fiber laser with CdS/PVA matrix thin film.

spectra from the output.

Results and discussion

The self-start pulse can be observed immediately once the QD CdS is incorporated into this cavity. Hence, no polarization controller is necessary to be applied in this configuration. The threshold lasing for continuous-wave without SA started at the pump power of 8.04 mW while the pulses for Q-switching started at a minimum pump power of 24.33 mW, which is lower than previous work [43–48]. Fig. 6(a) illustrates the spectrum of Q-switched fiber laser with the central wavelength of 1562 nm at the maximum pump power of 145.9 mW. Since the source power determines the spectrum, there are an obvious linewidth broaden observed while increasing the pump power. Fig. 6(b) shows a stable pulse train at the minimum pump power of 24.33 mW with a pulse repetition rate of 39.14 kHz and 26.0 μs response time. As the pump power is increased to 145.9 mW, the pulsed repetition rate increased to 75.19 kHz with 13.32 μs response time, as shown in Fig. 6(c). From Fig. 6(d), the single pulse for minimum and maximum pump power are merged in a graph to compare the pulse width, which reduced from 5.67 μs to 1.27 μs, respectively. An increase in pump power resulted in a higher repetition rate with a corresponding decrease in pulse width. Nevertheless, by comparing from other Q-switched fiber lasers with QD as SA, this is the shortest pulsewidth recorded as compare with QD CdSe [47] and PbS [44], which are reported to have 3.65 μs and 3.3 μs of pulsewidth, respectively. The pulse width could be reduced by optimizing parameters such as the performance of gain medium, lowering losses in the cavity, or enhancing the quality of CdS materials based on their properties [60].

The output laser versus time-dependent stability of Q-switched pulses is taken every five minutes for ten readings. The maximum pump power of 145.90 mW is used with a central wavelength of 1562 nm. The output spectra stability is shown in Fig. 7(a) where the output spectra are maintained during the operation, thus making it suitable for photonics applications. Meanwhile, the achieved signal-to-noise ratio (SNR) is depicted in Fig. 7(b) from the radio-frequency (RF) spectrum at ~40 dB. The fundamental frequency from RF spectra is ~75 kHz is corresponded with the pulse repetition rate perform at the maximum pump power of 145.9 mW. The relation of pulse repetition rate obtained for every pump power is observable from the RF spectrum analyzer.

Fig. 8(a) shows the relation of pulse repetition rate and pulse width versus pump power. The graph reveals that as the pump power increases from 24.33 mW to 145.9 mW, the pulse repetition rate value increases consistently, and the pulsewidth, conversely, decreases. These trends verified the Q-switched pulse' characteristics where the QD CdS saturated at a higher rate under a population inversion mechanism when increasing the pump power value [61]. Fig. 8(b) demonstrates a graph of average output power and pulse energy versus the laser diode pump power value. Both average output power and pulse energy increase as the pump power increases. These results indicates that when a higher pump power is injected into the system, it leads to a higher pulse energy, generated. The maximum pulse energy of 50.8 nJ is higher than those of Q-switched fiber laser using QD CdSe, as shown in Table 1.

Table 1 summarizes the synthesis method, integration platform, nonlinear characterization absorption, and laser properties for different types of QDs materials. In terms of the fabrication method for materials, QD CdS is synthesized via a microwave-assisted hydrothermal method, which is relatively easy, inexpensive, and faster fabricating process compared to the inverse micelle technique. Though inverse micelle

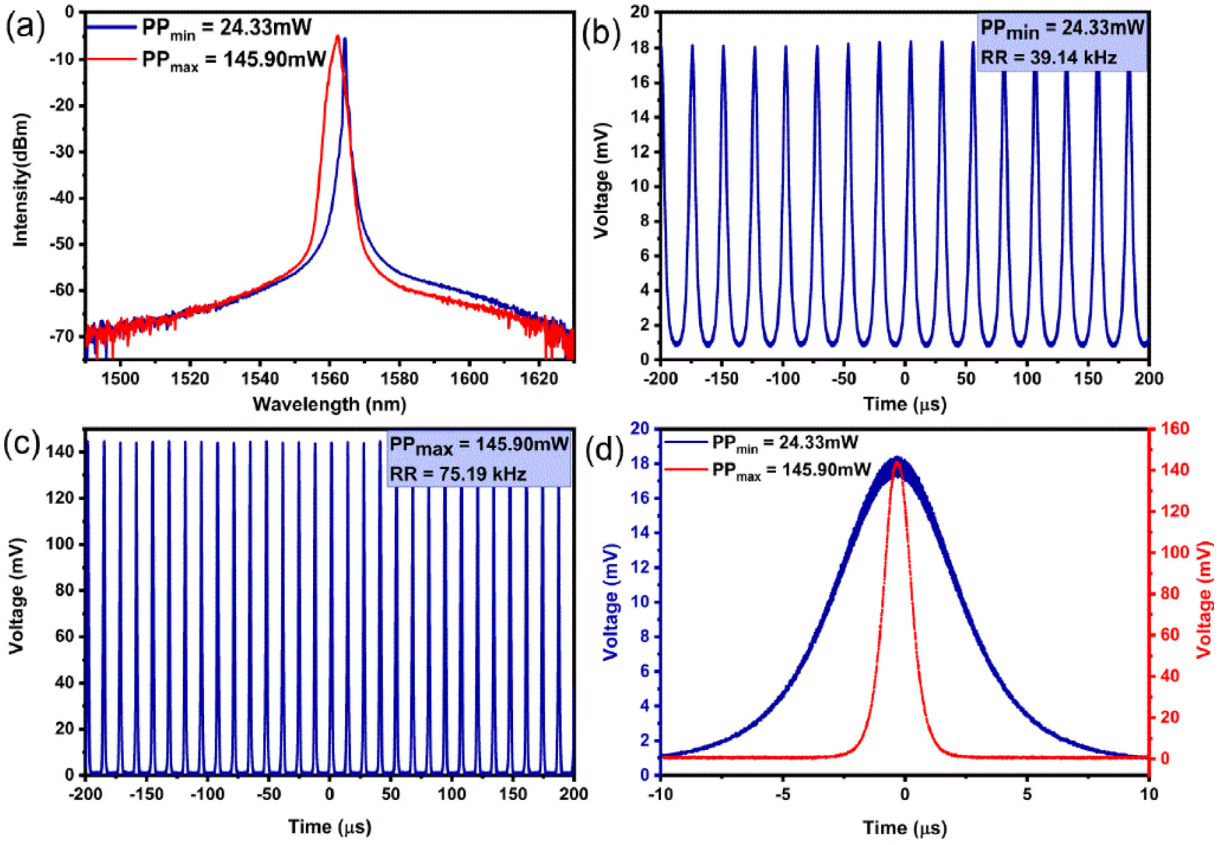

Fig. 6. Q-switched laser performances for (a) Output spectrum at maximum pump power, (b) Pulse train at minimum pump power, (c) Pulse train at maximum pump power, and (d) Single-pulse at a minimum and maximum pump power.

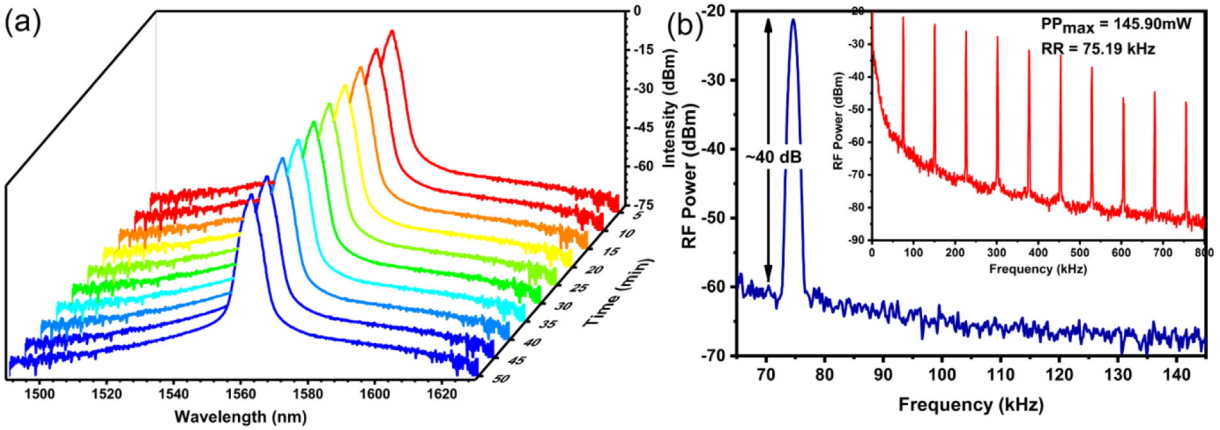

Fig. 7. (a) Stability of output spectra for the Q-switched pulsed at 5 min interval test period and (b) RF spectrum observed with maximum pump power at 145.9 mW.

technique has its advantage over the environmental preservation due to the absence of trioctylphosphine(TOP), it undergoes a complex synthesis process [54]. Although II-IV semiconducting material has been exploited as SA in the visible light region due to their strong photoluminescence and high resistance to photobleaching [57,62], yet there is none reporting research done on QD CdS at the infrared and near-infrared region. From the comparison table, the pulse width recorded in this work is the shortest as compare to other QD materials.

Conclusion

A Q-switched fiber laser with quantum dots CdS/PVA matrix film as the SA has been experimentally demonstrated with a central wavelength of 1562 nm generated by the EDF laser system. The QD CdS is synthesized via the microwave-assisted hydrothermal method and is embedded into polyvinyl alcohol (PVA) as the matrix film. The film is then sandwiched in between two fiber ferrules using an optical fiber adapter. The generation of Q-switched fiber laser with a repetition rate of 75.19 kHz, the pulse width of 1.27 μs, and the peak-to-peak pulse duration of 13.32 μs are successfully reported in this work. The maximum output power of 3.82 mW and maximum pulse energy of 50.8 nJ are achieved at the maximum pump power of 145.9 mW.

Declaration of Competing Interest

The authors declare that they have no known competing financial interests or personal relationships that could have appeared to influence the work reported in this paper.

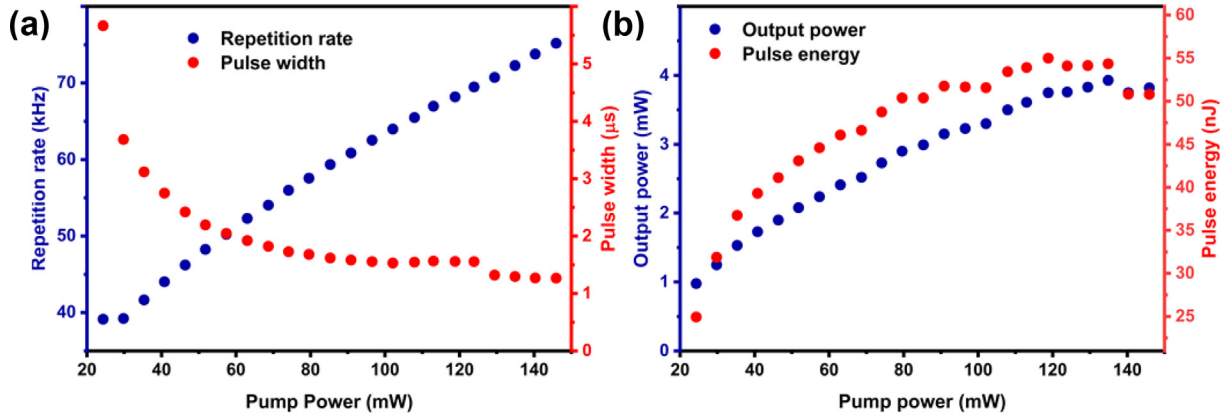

Fig. 8. (a) Pulse repetition rate and pulse width as a function of pump power and (b) average output power and pulse energy as a function of pump power.

Table 1
Comparison between Q-switched fiber laser with other QDs material.

QDs material	Synthesis method	Integration platform	Nonlinear characterization absorption		Laser type	Laser properties				Ref
			MD	I_{sat}		λ_c	RR	PW	E_{max}	
PbS	Wet chemical process	Microfiber	1.15%	–	EDFL	1533.04 nm	123 kHz	3.5 μs	121.2 nJ	[43]
		Fiber ferrule	6%	0.047 W/μm^2	EDFL	1562.7 nm	24.2 kHz	3.3 μs	801 nJ	[44]
		Fiber ferrule	5%	3.1 MW/cm^2	EDFL	1567.8 nm	68.04 kHz	3.9 μs	586.1 nJ	[45]
CdSe	Inverse micelle technique	Fiber ferrule	14.5%	10.8 MW/cm^2	YDFL	1081.5 nm	40.5 kHz	3.7 μs	1.1 μJ	[46]
		Fiber ferrule	11%	0.25 MW/cm^2	YDFL	1081 nm	40.5 kHz	3.65 μs	0.77 μJ	[47]
		Fiber ferrule	–	–	EDFL	1559.35 nm	68.45 kHz	4.3 μs	11.83 nJ	[48]
CdS	Microwave assisted Hydrothermal method	Fiber ferrule	19%	0.1570 MW/cm^2	EDFL	1562 nm	75.19 kHz	1.27 μs	50.8 nJ	[This work]

Acknowledgment

The authors would like to acknowledge the Ministry of Education Malaysia, for the project funds No. FRGS/2/2014/SG02/UPM/02/1/5524648 and FRGS/1/2018/STG02/UPM/02/1/5540123 that have been awarded to the authors in order to complete the research works.

Appendix A. Supplementary data

Supplementary data to this article can be found online at https://doi.org/10.1016/j.rinp.2020.103123.

References

[1] Stolow A, Bragg AE, Neumark DM. Femtosecond time-resolved photoelectron spectroscopy. Chem Rev 2004;104(4):1719–58.
[2] Zhang Q, Chang J, Wang Q, Wang Z, Wang F, Qin Z. Acousto-optic Q-switched fiber laser-based intra-cavity photoacoustic spectroscopy for trace gas detection. Sensors 2018;18(1):42.
[3] Ramakrishnan M, Rajan G, Semenova Y, Farrell G. Overview of fiber optic sensor technologies for strain/temperature sensing applications in composite materials. Sensors 2016;16(1):99.
[4] Hardy LA, Kennedy JD, Wilson CR, Irby PB, Fried NM. Analysis of thulium fiber laser-induced bubble dynamics for the ablation of kidney stones. J Biophotonics 2017;10(10):1240–9.
[5] Sen A, Doloi B, Bhattacharyya B. Fiber laser micro-machining of engineering materials. Non-traditional Micromachining Processes 2017:227–52.
[6] Tang Y, Xu J. A random Q-switched fiber laser. Sci Rep 2015;5:9338.
[7] Wang Y, Zhu X, Zong J, Wiersma K, Chavez-Pirson A, Norwood RA, et al. Q-switched fiber laser at 1.2 μm. CLEO 2016:1–2.
[8] Wang Y, Zhu X, Sheng C, Li L, Chen Q, Zong J, et al. SESAM Q-switched Ho^{3+}-doped ZBLAN fiber laser at 1190 nm. IEEE Photonic Tech L 2017;29(9):743–6.
[9] Zhang Z, Sang M, Ye Z, Nie Y. Passively Q-switched erbium-doped fiber laser based on nonlinear polarization rotation. Microw Opt Technol Lett 2008;50(3):694–6.
[10] Wang WB, Wang F, Yu Q, Zhang X, Lu YX, Gu J. Delivering dispersion-managed soliton and Q-switched pulse in fiber laser based on graphene and nonlinear optical loop mirror. Opt Laser Technol 2016;85:41–7.
[11] Nakazawa M, Yoshida E, Kimura Y. Low threshold, 290 fs erbium-doped fiber laser with a nonlinear amplifying loop mirror pumped by InGaAsP laser diodes. Appl Phys Lett 1991;59(17):2073–5.
[12] Kovalyov AA, Preobrazhenskii VV, Putyato MA, Pchelyakov OP, Rubtsova NN, Semyagin BR, et al. 115 fs pulses from Yb^{3+}: KY (WO_4) 2 laser with low loss nanostructured saturable absorber. Laser Phys Lett 2011;8(6):431.
[13] Venkatram N, Rao DN, Akundi MA. Nonlinear absorption, scattering, and optical limiting studies of CdS nanoparticles. Opt Express 2005;13(3):867–72.
[14] Chernysheva M, Mou C, Arif R, AlAraimi M, Rümmeli M, Turitsyn S, et al. High power Q-switched thulium-doped fiber laser using carbon nanotube-polymer composite saturable absorber. Sci Rep 2016;6:24220.
[15] Zou C, Yan Z, Huang Q, Wang T, Mou C, AlAraimi M. Wavelength switchable bi-directional Q-switched fiber laser based on 45° tilted fiber grating and carbon nanotube. BGPPM 2018:13.
[16] Yao BC, Rao YJ, Huang SW, Wu Y, Feng ZY, Choi C, et al. Graphene Q-switched distributed feedback fiber lasers with narrow linewidth approaching the transform limit. Opt Express 2017;25(7):8202–11.
[17] Huang B, Yi J, Du L, Jiang G, Miao L, Tang P, et al. Graphene Q-switched vectorial fiber laser with switchable polarized output. IEEE J Sel Top Quantum Electron 2016;23(1):26–32.
[18] Hou L, Sun J, Guo H, Lin Q, Wang Y, Bai Y, et al. High-efficiency, high-energy ytterbium-doped Q-switched fiber laser with graphene oxide-COOH saturable absorber. Laser Phys Lett 2018;15(7):075103.
[19] Ahmad H, Salim MAM, Thambiratnam K, Norizan SF, Harun SW. A black phosphorus-based tunable Q-switched ytterbium fiber laser. Laser Phys Lett 2016;13(9):095103.
[20] Liu H, Song W, Yu Y, Jiang Q, Pang F, Wang T. Black phosphorus-film with drop-casting method for high-energy pulse generation from Q-switched Er-doped fiber laser. Photonic Sens 2019:1–7.
[21] Wu K, Chen B, Zhang X, Zhang S, Guo C, Li C, et al. High-performance mode-locked and Q-switched fiber lasers based on novel 2D materials of topological insulators, transition metal dichalcogenides and black phosphorus: review and perspective. Opt Commun 2018;406:214–29.
[22] Haris H, Harun SW, Muhammad AR, Anyi CL, Tan SJ, Ahmad F, et al. Passively Q-switched Erbium-doped and Ytterbium-doped fiber lasers with topological insulator bismuth selenide (Bi2Se3) as saturable absorber. Opt Laser Technol 2017;88:121–7.
[23] Xu N, Ming N, Han X, Man B, Zhang H. Large-energy passively Q-switched Er-doped fiber laser based on CVD-Bi_2 Se_3 as saturable absorber. Opt Mater Express 2019;9(2):373–83.
[24] Li W, Peng J, Zhong Y, Wu D, Lin H, Cheng Y, et al. Orange-light passively Q-switched Pr 3+-doped all-fiber lasers with transition-metal dichalcogenide saturable absorbers. Opt Mater Express 2016;6(6):2031–9.
[25] Chen B, Zhang X, Wu K, Wang H, Wang J, Chen J. Q-switched fiber laser based on transition metal dichalcogenides MoS 2, MoSe 2, WS 2, and WSe 2. Opt Express 2015;23(20):26723–37.

[26] Niu K, Sun R, Chen Q, Man B, Zhang H. Passively mode-locked Er-doped fiber laser based on SnS_2 nanosheets as a saturable absorber. Photonics Res 2018;6(2):72–6.
[27] Zhang H, Liu J. Gold nanobipyramids as saturable absorbers for passively Q-switched laser generation in the 1.1 μm region. Opt Lett 2016;41(6):1150–2.
[28] Kang Z, Gao X, Zhang L, Feng Y, Qin G, Qin W. Passively mode-locked fiber lasers at 1039 and 1560 nm based on a common gold nanorod saturable absorber. Opt Mater Express 2015;5(4):794–801.
[29] Zhang H, Li B, Liu J. Gold nanobipyramids as a saturable absorber for passively Q-switched Yb-doped fiber laser operation at 1.06 μm. Laser Phys Lett 2017;14(2):025104.
[30] Xu N, Ma P, Fu S, Shang X, Jiang S, Wang S, et al. Tellurene-based saturable absorber to demonstrate large-energy dissipative soliton and noise-like pulse generations. Nanophotonics 2020.
[31] Kashiwagi K, Yamashita S. Optical deposition of carbon nanotubes for fiber-based device fabrication. Front Guided Wave Optics Optoelectron 2010;647.
[32] Wan H, Cai W, Wang F, Jiang S, Xu S, Liu J. High-quality monolayer graphene for bulk laser mode-locking near 2 μm. Opt Quant Electron 2016;48(1):11.
[33] Island JO, Steele GA, van der Zant HSJ, Castellanos-Gomez A. Environmental instability of few-layer black phosphorus. 2d Mater 2015;2(1):011002.
[34] Zunger A. Semiconductor quantum dots. MRS Bull 1998;23(2):15–7.
[35] Nozik AJ. Quantum dot solar cells. Physica E 2002;14(1–2):115–20.
[36] Towe E, Pan D. Semiconductor quantum-dot nanostructures: Their application in a new class of infrared photodetectors. IEEE J Sel Top Quantum Electron 2000;6(3):408–21.
[37] Shirasaki Y, Supran GJ, Bawendi MG, Bulović V. Emergence of colloidal quantum-dot light-emitting technologies. Nat Photonics 2013;7(1):13.
[38] Hetsch F, Zhao N, Kershaw SV, Rogach AL. Quantum dot field-effect transistors. Mater Today 2013;16(9):312–25.
[39] Cao Y, Wang C, Zhu B, Gu Y. A facile method to synthesis high-quality CdSe quantum dots for large and tunable nonlinear absorption. Opt Mater 2017;66:59–64.
[40] Mashford BS, Nguyen TL, Wilson GJ, Mulvaney P. All-inorganic quantum-dot light-emitting devices formed via low-cost, wet-chemical processing. J Mater Chem 2010;20(1):167–72.
[41] Valligatla S, Haldar KK, Patra A, Desai NR. Nonlinear optical switching and optical limiting in colloidal CdSe quantum dots investigated by nanosecond Z-scan measurement. Opt Laser Technol 2016;84:87–93.
[42] Xu Y, Wang Z, Guo Z, Huang H, Xiao Q, Zhang H, et al. Solvothermal synthesis and ultrafast photonics of black phosphorus quantum dots. Adv Opt Mater 2016;4(8):1223–9.
[43] Liu L, Sun X, Zhao W, Zhou B, Huang Q, Zou C, et al. Passively Q-switched pulses generation from Erbium-doped fiber laser based on microfiber coated PbS quantum dots. Opt Fiber Technol 2018;46:162–6.
[44] Lee YW, Chen CM, Huang CW, Chen SK, Jiang JR. Passively Q-switched Er^{3+}-doped fiber lasers using colloidal PbS quantum dot saturable absorber. Opt Express 2016;24(10):10675–81.
[45] Sun X, Zhou B, Zou C, Zhao W, Huang Q, Li N, et al. Stable passively Q-switched erbium-doped fiber laser incorporating a PbS quantum dots polystyrene composite film based saturable absorber. Appl Optics 2018;57(12):3231–6.
[46] Mahyuddin MBH, Latiff AA, Rusdi MFM, Irawati N, Harun SW. Quantum dot cadmium selenide as a saturable absorber for Q-switched and mode-locked double-clad ytterbium-doped fiber lasers. Opt Commun 2017;397:147–52.
[47] Hisyam MB, Rusdi MF, Latiff AA, Harun SW. PMMA-doped CdSe quantum dots as a saturable absorber in a Q-switched all-fiber laser. Chin Opt Lett 2016;14(8):081404.
[48] Ismail EI, Kadir NAA, Latiff AA, Arof H, Harun SW. Passively Q-switched erbium-doped fiber laser using quantum dots CdSe embedded in polymer film as a saturable absorber. Opt Quant Electron 2019;51(6):182.
[49] Ming N, Tao S, Yang W, Chen Q, Sun R, Wang C, et al. Mode-locked Er-doped fiber laser based on PbS/CdS core/shell quantum dots as saturable absorber. Opt Express 2018;26(7):9017–26.
[50] Huang S, Zhang Q, Huang X, Guo X, Deng M, Li D, et al. Fibrous CdS/CdSe quantum dot co-sensitized solar cells based on ordered TiO_2 nanotube arrays. Nanotechnology 2010;21(37):375201.
[51] Wang X, Qu L, Zhang J, Peng X, Xiao M. Surface-related emission in highly luminescent CdSe quantum dots. Nano Lett 2003;3(8):1103–6.
[52] Kharazmi A, Saion E, Faraji N, Soltani N, Dehzangi A. Optical properties of CdS/PVA nanocomposite films synthesized using the gamma-irradiation-induced method. Chin Phys Lett 2013;30(5):057803.
[53] Zhang P, Gao L. Synthesis and characterization of CdS nanorods via hydrothermal microemulsion. Langmuir 2003;19(1):208–10.
[54] Hamizi NA, Aplop F, Haw HY, Sabri AN, Wern AYY, Shapril NN, et al. Tunable optical properties of Mn-doped CdSe quantum dots synthesized via inverse micelle technique. Opt Mater Express 2016;6(9):2915–24.
[55] Wang Q, Geng B, Wang S. ZnO/Au hybrid nano architectures: wet-chemical synthesis and structurally enhanced photocatalytic performance. Environ Sci Technol 2009;43(23):8968–73.
[56] Malfatti L, Innocenzi P. Sol-gel chemistry for carbon dots. Chem Rec 2018;18(7–8):1192–202.
[57] Xu B, Luo S, Yan X, Li J, Lan J, Luo Z, et al. CdTe/CdS quantum dots: effective saturable absorber for visible lasers. IEEE J Sel Top Quant 2016;23(5):1–7.
[58] Koteswararao J, Satyanarayana SV, Madhu GM, Venkatesham V. Estimation of structural and mechanical properties of Cadmium Sulfide/PVA nanocomposite films. Heliyon 2019;5(6):e01851.
[59] Jeon J, Lee J, Lee JH. Numerical study on the minimum modulation depth of a saturable absorber for stable fiber laser mode-locking. J Opt Soc Am B 2015;32(1):31–7.
[60] Aldeek F, Balan L, Medjahdi G, Roques-Carmes T, Malval J, Mustin C, et al. Enhanced optical properties of core/shell/shell CdTe/CdS/ZnO quantum dots prepared in aqueous solution. J Physc Chem C 2009;113(45):19458–67.
[61] Zhang X, Li L, Zheng Y, Wang Y. The formation mechanism of optical bistability in end-pumped quasi-three-level Tm, Ho: YLF lasers. J Opt Soc Am B 2009;26(12):2434–9.
[62] Empedocles SA, Norris DJ, Bawendi MG. Photoluminescence spectroscopy of single CdSe nanocrystallite quantum dots. Phys Rev Lett 1996;77(18):3873.